

Survival of the fittest in the coherent evolution of quantum ensembles

G. Liu, O. Be'er, Y. Margalit, M. Givon, D. Groszwasser, Y. Japhay* and R. Folman
Department of Physics, Ben-Gurion University of the Negev, Beer-Sheva 84105, Israel.

(Dated: December 3, 2024)

We report two novel effects in an ensemble of two-level systems driven by an external field. First, we observe a frequency rigidity where the dominant Rabi oscillation frequency does not change with detuning, in contrast to the well-known law according to which the Rabi frequency grows with increasing detuning of the driving field. Second, we observe a time-dependent frequency shift of the ensemble-averaged oscillation, as some frequency components decay faster than others. Hence, coherence emerges from long-lived oscillations in an inhomogeneous ensemble. Our general model shows that these effects are related to a surprising double peak structure in the frequency spectrum of the generalized Rabi frequency. We show that the effects observed in alkali vapor are universal and expected in any system with a moderate inhomogeneity driven by an external field, and set stringent limits for applications requiring accurate coherent quantum manipulation.

I. INTRODUCTION

Rabi oscillations are an elementary process which is studied in a wide range of two-level systems driven by near resonant electromagnetic fields in the optical [1], micro-wave and radio-frequency regimes [2]. This process is of immense fundamental and technological significance [3–10] and consequently it is important that all its aspects be well understood. According to theoretical models, such as the Rabi or Jaynes-Cummings formalisms [3], the response of the system is described by the generalized Rabi frequency rule, stating that the oscillation frequency grows while the amplitude drops with increasing detuning of the driving field from the natural resonance of the two-level system. However, uncertainties and inhomogeneities in both the system and the field increase the complexity of the situation, giving rise to a rich spectrum of features.

Here we characterize and explain unique aspects of an ensemble of quantum two-level systems. Such ensembles are common in vapor, cold atom clouds, Bose-Einstein condensates, arrays of traps for cold ions and atoms, as well as related systems such as nitrogen-vacancy centers in diamonds.

Here we report on novel experimental observations related to the frequency of Rabi oscillations in an ensemble of atoms in a vapor cell, a system which is still of significant interest for applications in quantum science and technology [11–13]. We have measured the frequency of Rabi oscillations between two Zeeman sub-levels induced by a radio-frequency (RF) magnetic field and found that the oscillation frequency barely changes with the driving field's frequency, as shown in Fig. 1. This rigidity of the oscillation frequency seems to contrast the well-known rule of generalized Rabi frequency, according to which the oscillation frequency should grow with increasing detuning of the driving field frequency from the resonant

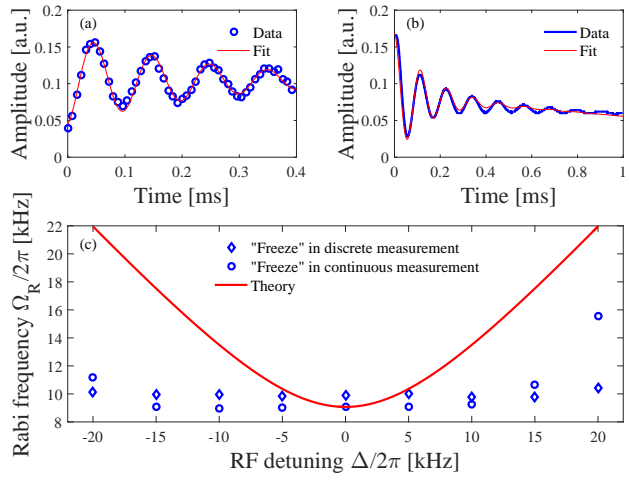


FIG. 1. (color online) Frequency rigidity of Rabi oscillations in a vapor cell (see section III). (a) Discrete measurement: Typical Rabi oscillations driven by an RF amplitude corresponding to a bare Rabi frequency $\Omega_0/2\pi \sim 10$ kHz. (b) Continuous measurement: Typical Rabi oscillations with a bare Rabi frequency $\Omega_0/2\pi \sim 9$ kHz. Red lines in (a) and (b) are single-frequency fits. (c) Rabi frequency vs. RF detuning. Red line in (c) is the expected generalized Rabi frequency according to $\Omega_R = \sqrt{\Omega_0^2 + \Delta^2}$, where Δ is the detuning. The rigidity is clearly visible.

transition frequency of the atoms. An analysis of this frequency rigidity, which we have observed for a wide range of parameters, shows that it originates from magnetic field inhomogeneity across the ensemble, even when the inhomogeneity is quite moderate (e.g. 0.05% measured inhomogeneity in our experiment). To the best of our knowledge, such a phenomenon was not previously reported or predicted. In addition to describing the observation in detail, we provide in the following a theoretical explanation and show that it is general, suggesting that the same phenomenon should be observable in any system involving driven oscillations of a two-level system in the presence of inhomogeneous broadening.

To emphasize the generality of the phenomenon, we

* Correspondence should be addressed to:
japhay@bgu.ac.il

start with a simple theory of Rabi oscillations in an inhomogeneous ensemble of two-level systems and show how Rabi frequency rigidity emerges from the interplay between inhomogeneous broadening of the transition (for which the resonance in our case is the Larmor frequency) across the ensemble and the driving rate of the ac field (bare Rabi frequency Ω_0). We then describe in detail the experimental observations and demonstrate the main effect predicted by the theory together with some related phenomena. In particular, a shift from high to low frequency during the Rabi oscillation is predicted by the theory and clearly observed experimentally for certain parameters. Our general model shows that this effect is universal and related to a surprising double peak structure in the frequency spectrum of the generalized Rabi frequencies. When inhomogeneous broadening is larger than the driving rate, the only frequency to survive in the long term is the lowest oscillation frequency, which is the bare Rabi frequency. This frequency, which has the lowest decay rate, is thus termed the fittest. This survival in the long term of one frequency component, may be viewed as the emergence of coherence in an inhomogeneous ensemble.

II. THEORY

A. Basic model

Consider a sample of many two-level atoms with an inhomogeneous energy splitting between their levels $|1\rangle$ and $|2\rangle$. The atoms are initially in level $|2\rangle$ and Rabi oscillations are induced by a driving field with a well-defined frequency detuned from the atomic transition frequency by δ . We assume that the value of δ varies across the sample due to the inhomogeneity of the transition frequency and has a distribution with an average $\langle\delta\rangle = \Delta$. The average detuning Δ can be controlled by varying the frequency of the driving field. For simplicity we assume a symmetric Gaussian distribution of δ with a spectral width σ . Our model has only three parameters: Δ , σ and the bare Rabi frequency Ω_0 determined by the driving field amplitude and the coupling of the field to an atom, which are assumed not to vary across the sample.

In the absence of inhomogeneity ($\sigma = 0$) we would expect the atoms in the sample to perform Rabi population oscillations between the two levels with the generalized Rabi frequency $\Omega_R = \sqrt{\Omega_0^2 + \Delta^2}$ and an amplitude Ω_0^2/Ω_R^2 (peak to peak). However, the integrated Rabi oscillation signal of an inhomogeneous sample, obtained by measuring the average population of the initially unpopulated level $|1\rangle$, is

$$P_1(t) = \frac{1}{2\sqrt{2\pi}\sigma} \int d\delta e^{-(\delta-\Delta)^2/2\sigma^2} \frac{1 - \cos[\omega(\delta)t]}{1 + \delta^2/\Omega_0^2}, \quad (1)$$

where $\omega(\delta) = \sqrt{\Omega_0^2 + \delta^2}$ is the generalized Rabi frequency for a atoms with a given δ . As noted, we model

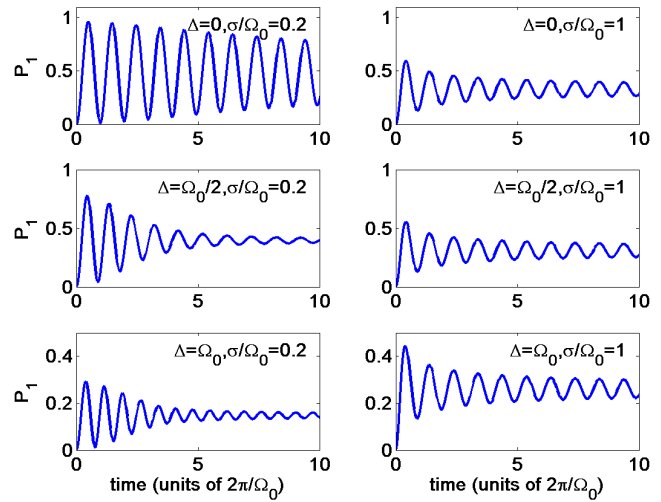


FIG. 2. (color online) Rabi population oscillations in an inhomogeneous ensemble calculated using the model in Eq. (1). If the inhomogeneous broadening (σ) is small relative to the driving rate (the bare Rabi frequency Ω_0) then the oscillation frequency Ω_R follows the $\Omega_R = \sqrt{\Omega_0^2 + \Delta^2}$ (“generalized Rabi frequency”) and grows with growing detuning Δ (left panel). However, if the inhomogeneous broadening is of the order of Ω_0 then the frequency of oscillation is dominated by the low frequency components and becomes the bare Rabi frequency (right panel). A closer look at the oscillations shows a shift from a higher frequency at short times to a lower frequency at long times. In addition, the decay of the oscillation is not exponential and the surviving oscillations after a long time have a very long decay time. These features are better analyzed by the two-frequency fit (section II B) or a Fourier transformation (section III).

the distribution of transition frequencies by a simple symmetric Gaussian function.

The integral in Eq. (1) is not in general solvable analytically. However, let us first consider a sub-sample of average detuning $\bar{\delta}$ and distribution of detuning frequencies $\xi = \delta - \bar{\delta}$ around $\bar{\delta}$ of width $\bar{\sigma}$. If the spectral width $\bar{\sigma}$ is much smaller than the bare Rabi frequency Ω_0 then the Lorentzian factor $(1 + \delta^2/\Omega_0^2)^{-1}$ in Eq. (1) can be taken out of the integral and the generalized Rabi frequency can be approximated by $\omega(\delta) \approx \bar{\Omega}_R + (\bar{\delta}/\bar{\Omega}_R)\xi$, where $\bar{\Omega}_R(\bar{\delta}) = \sqrt{\Omega_0^2 + \bar{\delta}^2}$. The partial signal from this sub-sample is then proportional to

$$\begin{aligned} & \frac{1}{1 + \bar{\delta}^2/\Omega_0^2} \int d\xi e^{-\xi^2/2\bar{\sigma}^2} [1 - \cos(\bar{\Omega}_R t + (\bar{\delta}/\bar{\Omega}_R)\xi t)] \\ & \propto \frac{1}{1 + \bar{\delta}^2/\Omega_0^2} \left[1 - \cos(\bar{\Omega}_R t) \exp\left(-\frac{\bar{\sigma}^2 \bar{\delta}^2}{2\bar{\Omega}_R^2} t^2\right) \right]. \end{aligned} \quad (2)$$

It follows that the contribution of a sub-sample, for which the driving field is detuned by $\bar{\delta}$, to the Rabi oscillation signal decays as $e^{-\gamma_{\bar{\delta}}^2 t^2/2}$, where the decay constant $\gamma_{\bar{\delta}}$ is proportional to $|\bar{\delta}|/\bar{\Omega}_R$. This decay is due to destructive interference between different frequency components within the same sub-sample. At short times the dominant oscillations are due to sub-samples with the highest

abundance of atoms, whose detuning is near the average detuning frequency Δ . However, after a long time the contribution of sub-samples with high detuning decays and the only oscillation frequencies that survive are those due to detunings near $\delta = 0$, whose decay constant is large. This gives rise to the frequency rigidity effect: as long as a sub-sample that is resonant with the driving field exists, its contribution to the Rabi oscillation signal is expected to be the dominant contribution after a long time, irrespective of the detuning of the driving field. Consequently, at long times, the only surviving Rabi oscillation is at the bare Rabi frequency. The above explanation also clarifies why one observes a change of the oscillation frequencies with time.

Note that the above explanation of the effect is only qualitative, as the division of the sample into subgroups is arbitrary. The spectral width of each sub-group and hence the decay rate of its partial signal is not uniquely determined and the actual mechanism of the formation of the signal involves interference between all the contributions from different atoms. A more rigorous explanation based on a numerical fitting procedure is presented below.

To demonstrate the effect we present in Fig. 2 calculated signals of Rabi oscillation that contain fast decaying frequency components and surviving frequency components that continue to oscillate at the bare Rabi frequency if the inhomogeneous spectral width σ is large enough compared to Ω_0 . This demonstrates the main effects reported in this paper and specifically the frequency rigidity at long times. A more detailed analysis of the theoretical model is given in section II B below.

In a practical system such as the one used in the experiment reported below, the model for the inhomogeneity may be more complex than the model presented above which contains only a single parameter σ for the width of the inhomogeneous broadening. In our experiment the inhomogeneity may be mainly attributed to the nonuniformity of the static magnetic field across the sample, which is responsible for a distribution of the Larmor frequency. The distribution of detuning frequencies in atoms contributing to the signal is also weighted by the location of the atoms across the probe beam that measures the atomic level population. In the next section we present, together with the experimental results, a more complex model for the inhomogeneity which also includes an asymmetric distribution (a skewed Gaussian). In addition, we take into account in a numerical model all the 5 atomic levels rather than only the two levels that are mainly occupied. The more detailed model reproduces the same phenomena that emerge from the simple model above: the Rabi frequency rigidity and the frequency shift during the oscillations, as observed in the experiment.

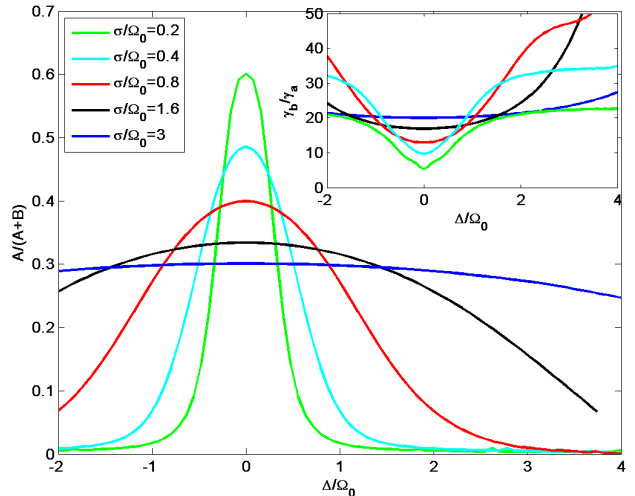


FIG. 3. (color online) A two-frequency model for the rigidity: fraction of the ensemble oscillating with the bare Rabi frequency Ω_0 vs. driving field detuning (in units of Ω_0) for varying inhomogeneity σ of the transition frequency (also in units of Ω_0). For $\sigma > \Omega_0$ the origin of the rigidity phenomenon becomes evident. Inset: Ratio between the decay rates of the low frequency part (γ_a) and the high frequency part (γ_b) of the Rabi oscillation as a function of the field detuning Δ at varying inhomogeneity σ .

B. Two-frequency fit

By performing the integral in Eq. (1) numerically we find that for almost the whole parameter space the oscillation signal can be very well fitted to a two-frequency model

$$P_1(t) \approx Ae^{-\gamma_a t} \cos(\Omega_0 t + \phi_a) + Be^{-\gamma_b t} \cos(\bar{\Omega} t + \phi_b), \quad (3)$$

representing two oscillation modes emerging from different parts of the sample: one with a low frequency Ω_0 and a slow decay rate γ_a , and one with a higher frequency $\bar{\Omega}$ and a fast decay rate γ_b ($\gamma_b \gg \gamma_a$). It follows that for a wide range of parameters Ω_0 , Δ and σ , the Rabi oscillation signal becomes after some time dominated by oscillations at approximately the bare Rabi frequency Ω_0 even if the expected “typical” oscillation frequency of the central part of the sample is the generalized Rabi frequency Ω_R , which may be much larger than Ω_0 for $\Delta > \Omega_0$.

To study the interplay between inhomogeneity and driving rate, we calculate the parameters of Rabi oscillations following from the fit in Eq. (3) for different ratios σ/Ω_0 . As shown in Fig. 3, when $\sigma \ll \Omega_0$ there is no rigidity as $A \rightarrow 0$; the fraction oscillating with Ω_0 is high only when the driving field frequency is near resonance, where $\Omega_R \approx \Omega_0$. However, when $\sigma > \Omega_0$ a large fraction of the ensemble oscillates with Ω_0 at any detuning and its oscillation, having a slow decay constant, completely dominates at longer times. In the inset we show that the ratio between the decay rates of the higher frequency oscillation mode and the oscillation at Ω_0 is always high, such that $\gamma_b \gg \gamma_a$ except when $\Delta \rightarrow 0$ and $\sigma \rightarrow 0$.

III. EXPERIMENT

A. The experimental setup

The experimental setup was presented previously in [15]. It is depicted here in Fig. 4. While we describe the setup and the observations it gave rise to, it is important to emphasize yet again that the main phenomenon reported here (rigidity of the oscillation frequency) is not unique to this setup and represents a general physical effect.

We induce Rabi population oscillations in a ^{87}Rb vapor contained in a cylindrical ($\varnothing 25 \times 38$ mm) cell with neon buffer gas at room temperature and 75 Torr. The thermal relaxation time of the ground state magnetic polarization (T_1) for the rubidium atoms in this cell in the absence of light is measured to be about 30 ms [14]. Since the duration of the experiment (~ 1 ms) is much shorter, interpreting the observed phenomena does not rely on the specific properties of the vapor. Indeed, we observed the rigidity phenomenon with different buffer gases and varying pressures (Ne at 7.5 and 75 Torr, and Kr at 60 Torr), data which will not be described here in detail.

The two-level system used for the Rabi oscillation is a system of Zeeman sub-levels of the hyperfine level $F = 2$ that were energetically split in a static magnetic field, produced by several sets of Helmholtz coils. We exploit the nonlinear Zeeman effect to isolate two of the Zeeman sub-levels from the others, such that transitions are induced only between the sub-levels $|F, m_F\rangle = |2, 2\rangle$ and $|2, 1\rangle$. This is facilitated by a magnetic field of about 26 G, strong enough to shift transitions other than the one under investigation by about 100 kHz. Three mutually perpendicular sets of square Helmholtz compensation coils cancel Earth's magnetic field. The z bias coils produce the 26 G DC magnetic field parallel to the axis of the vapor cell, while the auxiliary y coils produce a 1 G magnetic field in the y direction.

A RF magnetic field perpendicular to the vapor cell axis (quantization axis) for driving the transitions between the Zeeman sub-levels $|2\rangle \equiv |2, 2\rangle$ and $|1\rangle \equiv |2, 1\rangle$ is produced by the RF coils. The driving rate (bare Rabi frequency) is $\Omega_0 = g_F \mu_B \langle 1 | \hat{F}_\perp | 2 \rangle B_{\text{RF}} / \hbar$, where μ_B is the Bohr magneton, $g_F \approx 1/2$ is the Landé factor for the hyperfine level $F = 2$, B_{RF} is the amplitude of the oscillating magnetic field and $\langle 1 | \hat{F}_\perp | 2 \rangle = 1$ is the matrix element of the perpendicular component of the total angular momentum $\mathbf{F} = \mathbf{L} + \mathbf{S} + \mathbf{I}$ between the two Zeeman sub-levels. We limit Ω_0 to a maximum of 25 kHz, thereby keeping the two-photon transition rate to $|2, 0\rangle$ negligible.

Pumping the atoms into the desired levels is done by two circularly polarized lasers tuned to the $F=1 \leftrightarrow F'=2$ transition in the D₂ line (marked in blue) and to the $F=2 \leftrightarrow F'=2$ transition in the D₁ line (marked in green). The two beams are combined by beam splitter BS4, and the quarter-wave plate makes their polarization circular. The pump beams' intensities are controlled by a neutral den-

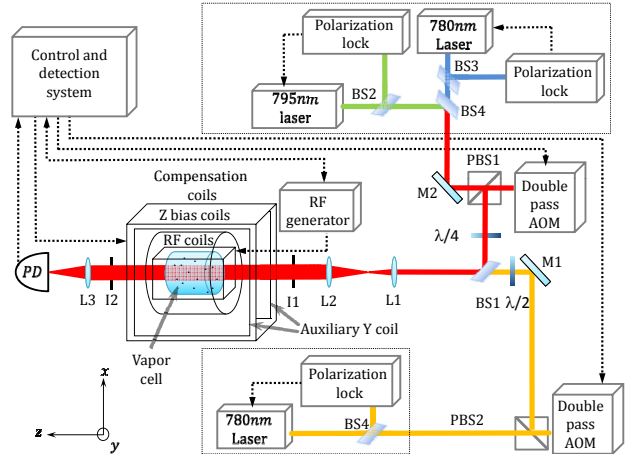


FIG. 4. (color online) Experimental setup. BS1, BS2, BS3 and BS4 are beam splitters; PBS1 and PBS2 are polarizing beam splitters; L1, L2 and L3 are lenses; I1 and I2 are irises; M1 is a mirror and PD is a photo-diode. Dashed lines indicate data and control lines. The double-pass AOM can turn the laser beams on and off within 1 μs . The lenses L1 and L2 and the iris I1 control the diameter and the intensity profile of the beam.

sity filter (not shown). The $|2, 2\rangle$ Zeeman sub-level is a dark state for both beams when the circular polarization is right-handed, while the $|2, -2\rangle$ sub-level is a dark state for left-handed circular polarization. When both beams are turned on, they can pump 95% of the ^{87}Rb atoms to the $|2, 2\rangle$ sub-level (or to $|2, -2\rangle$) within 50 μs (or longer, as needed).

The probe laser is tuned to a frequency of about 200 MHz above the $F=2 \leftrightarrow F'=2$ transition in the D₂ line (marked in yellow) and a half-wave plate is set to fix the probe beam polarization in the y direction. When the magnetic field is in the y direction, the probe beam can induce only π transitions. Under such conditions and at that frequency, the optical density of the vapor is sensitive to the distribution of the population between the $|2, 2\rangle$ and $|2, 1\rangle$ sub-levels [15].

The probe beam is combined with the pump beams by BS1. The beams are expanded by a telescope, traverse the vapor cell, and then focused on a photo-diode (PD). The intensity of the light incident on the PD is recorded as a function of time.

The control system allows the creation of a variety of sequences combining beams, DC and RF magnetic fields, triggering of the PD recording, etc. Here we present two such sequences, implemented in this paper as the two methods for inducing and observing Rabi oscillations [14].

In this work, all experimental data are based on the $|2, 1\rangle \leftrightarrow |2, 2\rangle$ transition unless otherwise specified.

B. Experimental procedure

We use two methods to observe Rabi oscillations [14]:

Method 1: Discrete measurement. We turn on the DC magnetic field and pump most of the population to the $|2, 2\rangle$ state. We then turn off the pumping beams and turn on the RF field for a duration t to induce Rabi oscillations. Turning on the probe beam, tuned to about 200 MHz above the $F=2 \rightarrow F'=2$ transition in the D_2 line, probes the Rabi oscillations between these two states [15]. We repeat this process n times (typically $n=50$), each time increasing the duration t by Δt (typically $\Delta t=8 \mu\text{s}$).

Method 2: Continuous measurement. We turn on the DC magnetic field and pumping laser beams, and then turn on the RF field. With a bandpass filter, only the power of the 795 nm (D1) circularly polarized pumping laser beam passing through the vapor cell is registered by a photodetector. This beam also acts as a probe beam (while the RF is still on). As the state $|2, 2\rangle$ is a dark state for this beam while $|2, 1\rangle$ is not, the beam's intensity after passing through the ensemble reflects the population difference.

Although in the first method only the RF radiation interacts with the atoms during the oscillations while in the second there are two additional light fields, we have verified that the rigidity phenomenon is observed with both methods, as shown by Fig. 1(c). In order to quicken data taking thus reducing experimental drifts, we utilize the continuous method throughout this work.

C. Results: Rabi frequency rigidity

Figures 1(a-b) show the raw data of Rabi oscillations obtained with the above two methods. We extract the Rabi frequency ω at each RF detuning, as shown in Fig. 1(c), by fitting the data to a function $Ae^{-\gamma t} \cos(\omega t + \phi) + Bt + C$, where A is the oscillation amplitude, ϕ is the initial phase, γ is the exponential decay rate, B is the drift coefficient of the signal, and C is its baseline. The fitting window is $0.01 \text{ ms} < t < 0.6 \text{ ms}$, long enough as the oscillations usually vanish before $t=0.6 \text{ ms}$.

We compare the measured Rabi frequency derived from the single frequency fit to the oscillation frequency predicted for a homogeneous sample with the same central detuning Δ . As noted, Ω_R should grow with increasing Δ . However, in contrast and as shown in Fig. 1(c), we have unveiled a regime in which the Rabi frequency hardly changes with RF frequency, thereby giving rise to a frequency rigidity.

We study this frequency rigidity over a range of RF amplitudes and DC magnetic field inhomogeneity. Figs. 5(a) and (b) show the observed Rabi frequency for larger and smaller magnetic field inhomogeneity, respectively, as a function of the RF detuning Δ from the overall resonance frequency of the ensemble. This overall resonance frequency is determined by measuring the pump beam transmission while scanning the RF slowly. We

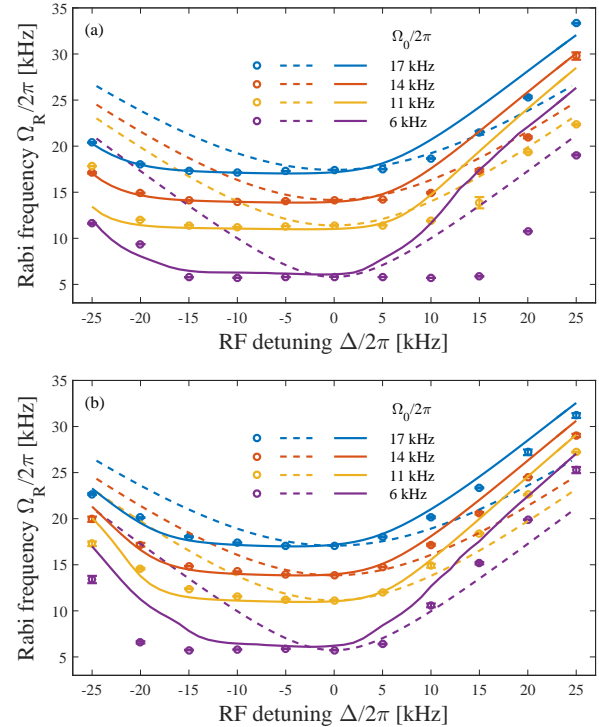


FIG. 5. (color online) Rigidity of Rabi oscillation for large and small inhomogeneity: experiment (circle) vs. numerical model (solid line); dashed lines show the expected $\Omega_R = \sqrt{\Omega_0^2 + \Delta^2}$. (a) Large magnetic field inhomogeneity (12 mm probe beam diameter). (b) Small field inhomogeneity (3 mm diameter). The numerical model assumes a skewed Gaussian distribution of the magnetic field with widths $\sigma/2\pi=10 \text{ kHz}$ and 8 kHz for (a) and (b), respectively. In both cases, the skewing is represented by a Gauss error function characterized by $\text{erf}(-0.3/\sqrt{2}) \sim 23.6\%$, and the homogeneous decoherence rate is $\gamma/2\pi=1 \text{ kHz}$.

vary the inhomogeneity by using different beam diameters (12 and 3 mm), as reduced diameter beams pump and probe smaller parts of the ensemble, therefore suffering smaller variations of the magnetic field. Qualitatively, one may observe that the rigidity phenomenon increases with increasing inhomogeneity and decreases with increasing bare Rabi frequency (e.g. see purple data for strongest rigidity). In Figs. 5(a-b) there is an apparent asymmetry of the frequency rigidity between red and blue detuning. This is due to an asymmetric inhomogeneity of the magnetic field, as discussed below when describing our numerical model.

A phenomenon directly related to the frequency rigidity is a shift from higher to lower oscillation frequency during the oscillation, as predicted in section II. This phenomenon appears more clearly in our measurements for certain experimental parameters, as demonstrated in the inset of Fig. 6(a), for red detuning and a 3 mm probe beam. We observe a frequency shift, where at first the

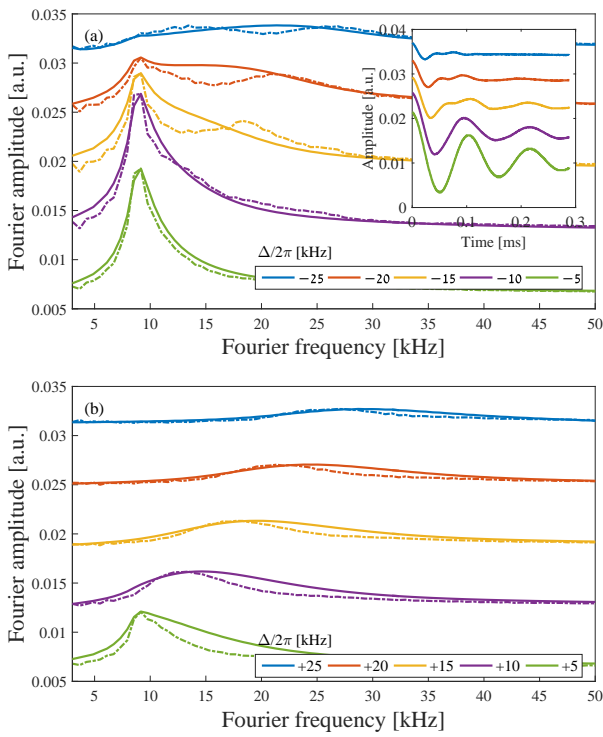


FIG. 6. (color online) Fourier analysis of the observed Rabi oscillations: experiment (dashed-dotted line) vs. numerical model (solid line) for a red (a) and blue (b) detuned RF field. In (a) the Fourier spectra shows a double peak structure. As explained in the text, the two peaks correspond to two oscillation modes: high frequency - fast decaying, and low frequency - slow decaying. These cause the time-domain frequency shift shown in the inset of (a). The rigidity is presented in (a) by a sharp peak at $\Omega_0/2\pi \sim 9$ kHz, unchanged regardless of the increasing Δ . Parameters used in the numerical model are the same as for Fig. 5(b). Each Fourier curve is displaced vertically for clarity of presentation.

Rabi oscillations have a high frequency and then after a few cycles a lower frequency dominates. We analyze the data by a Fourier transform, which is shown in Fig. 6(a) (dashed-dotted lines). The two-peak structure demonstrates the frequency shift mentioned above. The rigidity is due to the dominance of the low frequency component, which maintains the same frequency (bare Rabi frequency) independent of the detuning. In contrast, in Fig. 6(b), the Fourier spectra of blue-detuned Rabi oscillations show that the rigidity disappears, as in Fig. 5. Solid lines in Fig. 6 (main panels) show the numerical results (discussed in the following).

The experimental observations described above indicate that greater inhomogeneity strengthens the rigidity, while the rigidity weakens with larger RF (driving field) power. An inhomogeneity of 10 kHz, (corresponding to the independently measured inhomogeneity of 15 mG out of 26 G [16]) fits the experimental results for the 12 mm beam (Fig. 5). For the 3 mm beam, the best-fit inho-

mogeneity is only reduced to 8 kHz (less than the 4-fold decrease from 12 to 3 mm) since the inhomogeneity is mostly along the axial direction of the cell. Reducing the beam diameters further is impractical, due to a decrease of the observable signal. One may also consider reducing the rigidity by increasing the driving field amplitude instead, which however leads in our specific case to a breakdown of the two-level approximation by introducing a two-photon transition to a third level. It should be noted that in our experiment the driving field has a measured inhomogeneity of $\sim 2\%$ across the atom-field interaction region, meaning a < 400 Hz deviation of the bare Rabi frequency. This is much smaller than the inhomogeneous broadening (which is of the order of Ω_0), thus having a negligible effect on the phenomena observed here.

D. Comparison with a numerical model

The theoretical model presented in section II reproduces qualitatively the main results observed in our experiment, namely: rigidity of the oscillation frequency and a shift from higher to lower frequency during the oscillation. However, in order to produce a theory with results comparable quantitatively to our observations we introduce a detailed numerical model that takes into account the full Zeeman level system and uses an asymmetric model for the inhomogeneity, which can account for the asymmetry reported above between red and blue detuned driving frequencies. We numerically solve the master equations for the five Zeeman sub-levels of the $F=2$ hyperfine state exposed to an RF field and a DC magnetic field. We obtain the time evolution of the population in the $|2, 2\rangle$ state, for changing RF detuning Δ , RF power parameterized by the bare Rabi frequency Ω_0 , and changing DC magnetic field inhomogeneity parameterized by the width σ of a Gaussian distribution describing the fraction of atoms for each value of the inhomogeneous DC magnetic field. We then fit curves of the population vs. time (single-frequency fit as for the experimental data) to extract the Rabi oscillation frequency ω for various Δ , Ω_0 and σ . To explain the asymmetry of the rigidity with respect to detuning (Fig. 5), we introduce into the numerical model a DC magnetic field asymmetry in the form of a skewed Gaussian. Such asymmetry could be caused by a magnetic field inhomogeneity that is not symmetric relative to the cell center (see section IV). Good qualitative agreement is achieved.

We analyze the numerical results by Fourier transform. The solid lines in Fig. 6 show that the model qualitatively agrees with the experiment. The two-peak structure in the numerical results is not as clear as in the experimental data (dashed-dotted lines). We believe that the discrepancy is due to a complicated magnetic field distribution, which could not be simulated by our simple model. The numerical results teach us that in general the frequency shift occurs for a wide range of parameters and may be either fast or slow. However, due to our

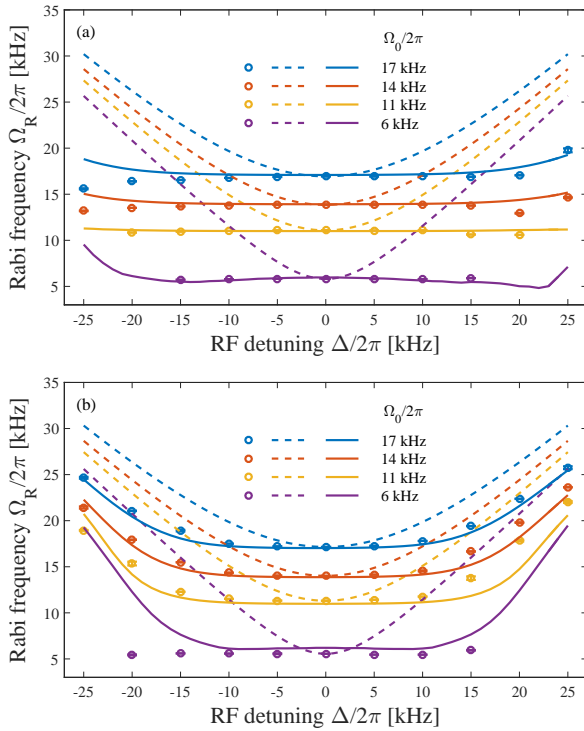


FIG. 7. (color online) Rigidity of the Rabi oscillation frequency for large and small inhomogeneity in the $|2, -2\rangle \leftrightarrow |2, -1\rangle$ transition. Presented are the experimental results (circles), the expected $\Omega_R = \sqrt{\Omega_0^2 + \Delta^2}$ (dashed line) and the numerical model (solid line). (a) Large magnetic field inhomogeneity (beam diameters of 12 mm). (b) Small field inhomogeneity (beam diameters of 3 mm). The numerical model assumes a symmetric Gaussian distribution of the magnetic field with widths $\sigma/2\pi = 12$ kHz and 8 kHz for (a) and (b), respectively, and a homogeneous decoherence rate of $\gamma/2\pi = 1$ kHz.

limited signal-to-noise ratio we were able to observe it clearly in the experiment only for the case of small inhomogeneity (3 mm beam) and red-detuned RF, as shown in the inset of Fig. 6(a).

IV. ASYMMETRY EFFECT

In this section we briefly present and explain the effect of asymmetry observed in Fig. 5. We believe that this is not a fundamental effect as, for example, it is hardly observable in the $|2, -2\rangle \leftrightarrow |2, -1\rangle$ transition, as described in the following. Instead, as shown, it stands to reason that the effect follows from a specific configuration of the experimental setup responsible for a different magnetic field distribution across the cell in the two measurement configurations. For completeness we present these results here.

Figure 5 shows that the frequency of Rabi oscillations between the sub-levels $|2, 2\rangle$ and $|2, 1\rangle$ behaves in a dif-

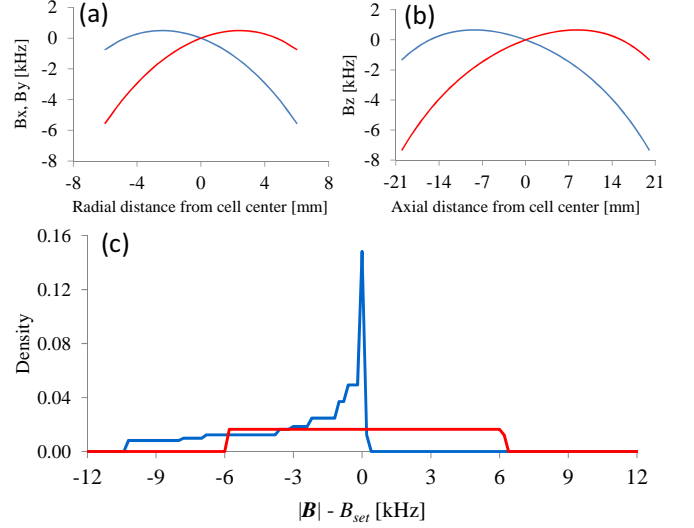


FIG. 8. (color online) (a-b) An example for the possible dependence of the components of the DC magnetic field (in kHz, 10 mG = 7 kHz) inside the cell as a function of position. (a) Radial components: blue line - $B_{0x,y}$; red line - $B_{1x,y}$ (see text). (b) Axial components: blue line - B_{0z} ; Red line - $B_{1z} - B_{set}$. (c) Distribution of the magnetic field deviation (in kHz, 10 mG = 7 kHz). Red - $|\mathbf{B}_{tot+} - B_{set}|$. (Average 0.1 kHz, 49.4% below average, 50.6% above average); Blue - $|\mathbf{B}_{tot-} - B_{set}|$. (Average -3.16 kHz, 42% below average, 58% above average).

ferent way for red and blue detuning. For comparison, we present in Fig. 7 a similar plot for the transition $|2, -2\rangle \leftrightarrow |2, -1\rangle$, in which the asymmetry between red and blue detuning is very slight.

A possible explanation for the difference between the asymmetry in the two transitions lies in the magnetic configuration used for each of them. Switching between these configurations is done by reversing the current in the z -axis bias coils (see Fig. 4). As demonstrated below, reversing the current can change the magnetic field distribution around its target value B_{set} . The symmetry of the magnetic field distribution, which was modeled by skewness of the Gaussian distribution in our numerical model used for fitting the experimental results, determines also the symmetry or asymmetry of the Rabi frequency dependence on the detuning, as demonstrated in Fig. 7 (symmetric) and Fig. 5 (asymmetric).

The details of the deviation of the magnetic field from its target value are unknown to us. However, we can use a simple model to demonstrate how the symmetry of the distribution can change when the magnetic field due to the current in the z bias coils is reversed. In general, the magnetic field is a sum of two parts: the field $\mathbf{B}_0 \sim (0, 0, 0)$ due to earth and the compensation coils and $\mathbf{B}_1 \sim (0, 0, \pm B_{set})$ due to the z bias coils. Our model assumes for simplicity that each component B_x, B_y and B_z of the two parts of the field varies only along the respective directions x, y and z ($-20 \text{ mm} < z < 20 \text{ mm}$ along the axis of the cell and $-8 \text{ mm} < x, y < 8 \text{ mm}$ along

the transverse direction).

The field components for this example are presented in Fig. 8(a-b). The magnetic field is given in units of kHz (700 kHz/G). The variation of the magnetic field is well within ± 8 kHz ($\pm 0.05\%$ of B_{set}). The distributions of the values of the total magnetic field $|\mathbf{B}_{tot\pm}| = |\mathbf{B}_0 \pm \mathbf{B}_1|$ calculated at a grid of points (spacing: 0.5 mm) in the active volume of the vapor cell are presented in Fig. 8(c). Clearly, reversing the current can change a symmetric distribution to a skewed one.

Finally, the asymmetry effect may be related to another observation made in the process of measuring the atomic population while slowly scanning the RF frequency in the presence of the DC magnetic field and the pumping beams (method 2 described in section III B). The RF frequency was scanned during 1 s in a window of ± 100 kHz across the resonance transition frequency as initially calculated from the estimated DC magnetic field in the vapor cell. Figure 9(a) presents such spectra for the $|2, 2\rangle \leftrightarrow |2, 1\rangle$ transition at various values of the RF power, and Fig. 9(b) presents similar spectra for the $|2, -2\rangle \leftrightarrow |2, -1\rangle$ transition. The spectra represent the pump beam transmission for the steady-state optical density in the presence of both a pump and a driving RF field. We define the resonant transition frequency to be used as the reference frequency throughout this work as the RF frequency at the minimum of the spectrum measured for a RF power corresponding to a Rabi frequency of $\Omega_0/2\pi = 9$ kHz. In our setup, we find the resonance frequency to be 18.167 MHz for the $|2, 2\rangle \leftrightarrow |2, 1\rangle$ transition and 18.481 MHz for the $|2, -2\rangle \leftrightarrow |2, -1\rangle$ transition. As seen by zooming-in on the dips, the position of the minimum changes with RF power. We have fitted a Voigt profile [17] to the spectra to locate the exact value of the minima and find that they are detuned from resonance by -2 to 0.5 kHz for the $|2, 2\rangle \leftrightarrow |2, 1\rangle$ transition and by -1.1 to 0.8 kHz for the $|2, -2\rangle \leftrightarrow |2, -1\rangle$ transition.

These slight changes in the resonance frequency and the detunings of the minima again indicate that the magnetic field in both configurations is different. The detailed modelling and understanding of these slight changes is beyond the scope of this paper, as it requires exact knowledge of the magnetic field which is not available to us.

V. OUTLOOK AND CONCLUSIONS

Here we have described a general phenomenon that is likely to appear in many kinds of inhomogeneous systems performing driven oscillations. If the dependence of the oscillation frequency Ω on the inhomogeneous factor (let us call it η) that varies across the sample has an extremum at a given value of η , where $\partial\Omega/\partial\eta = 0$, then an effect of frequency rigidity similar to what we observed in this work may appear. The overall (average) oscillation signal in the long time range would then become dominated by a single frequency that does not change if the

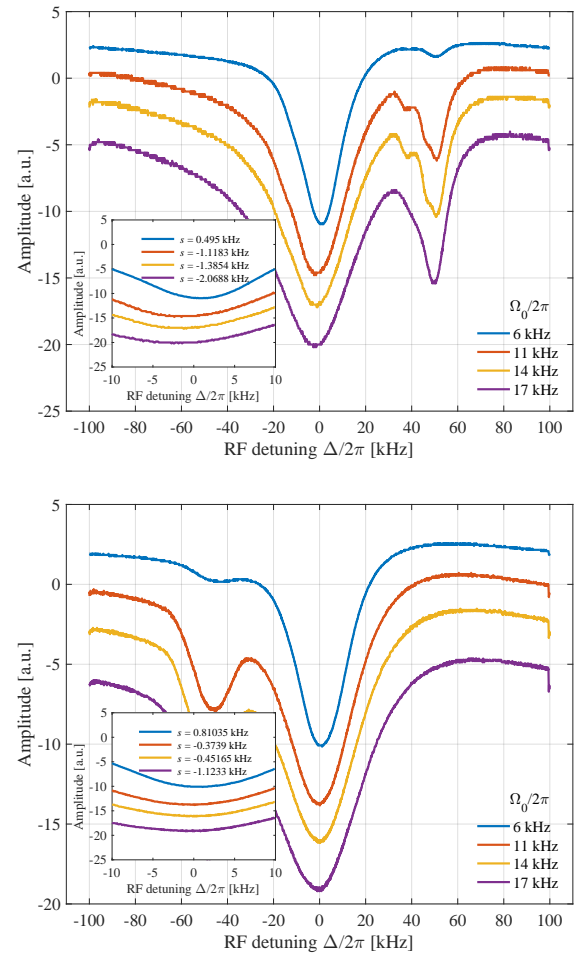


FIG. 9. (color online) Spectra of the laser power exiting the vapor cell as a function of the detuning Δ . The RF power level for each spectrum is given by the Rabi frequency it induces (Ω_0). The main dip in (a) represents the $|2, 2\rangle \leftrightarrow |2, 1\rangle$ transition (18.167 MHz) and in (b) the transition $|2, -2\rangle \leftrightarrow |2, -1\rangle$ (18.481 MHz). The smaller dip at a detuning of ± 50 kHz in (a) and (b) is the two-photon $|2, \pm 2\rangle \leftrightarrow |2, 0\rangle$ transition. The spectra are shifted from each other in the vertical direction for clarity. In the inset we present a zoom-in on the dip area, and list the deviations s of the dips associated with different RF power.

inhomogeneous factor η is shifted over the whole sample. We have demonstrated this frequency rigidity for Rabi oscillations where the detuning parameter, which is controlled by the frequency of the external driving field, is varying across the sample. The rigidity effect follows from the fact that the dependence of the Rabi frequency on the detuning δ has a minimum at $\delta = 0$, as explained in section II, giving rise to rigidity at the bare Rabi frequency.

We have shown theoretically and experimentally how the frequency rigidity effect emerges from the interplay between driving rate and inhomogeneous broadening and analyzed in detail some more specific features

of this phenomenon. Our analysis provides a quantitative guide concerning the interplay between inhomogeneity and driving rate (driving field power). The effects are universal and do not depend on the specific type of two-level system, the origin of inhomogeneity of the resonance frequency, or the specific form of interaction with the driving field. In devices for which miniature dimensions are required, as well as fast operations, keeping clear of the restrictions described here may not be easy to achieve.

Some surprising protocols may arise; for example, in the case of an inhomogeneity that cannot be suppressed to a low enough level, it is advantageous to increase the inhomogeneity so that γ_b becomes larger and

the Rabi oscillation becomes monochromatic (bare frequency) faster (although the signal becomes weaker in analogy to “Doppler-free” spectroscopy). This gives, for example, an accurate measure of the driving field intensity at the position of the ensemble.

ACKNOWLEDGMENTS

We thank Mark Keil for his critical reading of the manuscript. This work is funded in part by the Israeli Science Foundation, the EC Matter–Wave consortium (FP7-ICT-601180), and the German-Israeli DIP project (Hybrid devices: FO 703/2-1) supported by the DFG.

[1] P. Knight and P. Milonni, *Physics Reports* **66** (1980).

[2] L. M. K. Vandersypen and I. L. Chuang, *Rev. Mod. Phys.* **76**, 1037 (2005).

[3] D. G. Andrew, K. Jens, and L. Jonas, *Journal of Physics B: Atomic, Molecular and Optical Physics* **46**, 220201 (2013).

[4] D. Budker and M. Romalis, *Nature Physics* **3**, 227 (2007).

[5] F. Jelezko, T. Gaebel, I. Popa, M. Domhan, A. Gruber, and J. Wrachtrup, *Phys. Rev. Lett.* **93**, 130501 (2004).

[6] D. Press, T. D. Ladd, B. Zhang, and Y. Yamamoto, *Nature* **456**, 218 (2008).

[7] A. Palacios-Laloy, F. Mallet, F. Nguyen, P. Bertet, D. Vion, D. Esteve, and A. N. Korotkov, *Nature Physics* **6**, 442 (2010).

[8] Y. Dudin, L. Li, F. Bariani, and A. Kuzmich, *Nature Physics* **8**, 790 (2012).

[9] R. Vijay, C. Macklin, D. H. Slichter, S. J. Weber, K. W. Murch, R. Naik, A. N. Korotkov, and I. Siddiqi, *Nature* **490**, 77 (2012).

[10] N. Navon, S. Kotler, N. Akerman, Y. Glickman, I. Almog, and R. Ozeri, *Phys. Rev. Lett.* **111**, 073001 (2013).

[11] W. Wasilewski, K. Jensen, H. Krauter, J. J. Renema, M. V. Balabas, and E. S. Polzik, *Phys. Rev. Lett.* **104**, 133601 (2010).

[12] H. Krauter, D. Salart, C. Muschik, J. M. Petersen, H. Shen, T. Fernholz, and E. S. Polzik, *Nature Physics* **9**, 400 (2013).

[13] T. Baluksian, B. Huber, R. Löw, and T. Pfau, *Phys. Rev. Lett.* **110**, 123001 (2013).

[14] O. Be'er, *Transitions between atomic quantum levels in room temperature ^{87}Rb vapor*, Master's thesis, Ben-Gurion University of the Negev (2016).

[15] M. Givon, Y. Margalit, A. Waxman, T. David, D. Groswasser, Y. Japha, and R. Folman, *Phys. Rev. Lett.* **111**, 053004 (2013).

[16] M. Givon, *A Magic Frequency in Light-Matter Interaction of a Two-State System with Multiple Degeneracy*, Ph.D. thesis, Ben-Gurion University of the Negev (2015).

[17] M. D. Rotondaro and G. P. Perram, *Quant. Spectrosc. Radiat. Transfer* **57**, 497 (1997).